Calculation of the shear viscosity of decane using a reversible multiple time-step algorithm

Cite as: J. Chem. Phys. **102**, 3376 (1995); https://doi.org/10.1063/1.469211
Submitted: 31 August 1994 • Accepted: 11 November 1994 • Published Online: 04 June 1998

Christopher J. Mundy, J. Ilja Siepmann and Michael L. Klein

Calculation of the shear viscosity of decane using a reversible multiple time-step algorithm

Christopher J. Mundy, J. Ilja Siepmann,[a] and Michael L. Klein
Department of Chemistry, University of Pennsylvania, Philadelphia, Pennsylvania 19104-6323

(Received 31 August 1994; accepted 11 November 1994)

The shear viscosity of a fully-flexible model for *n*-decane is calculated via equilibrium molecular dynamics simulations at the state point $T=480$ K and $\rho=0.6136$ g/cm^3. A reversible multiple-time step approach is used in conjunction with Nosé–Hoover chain dynamics to generate data in the canonical (NVT) ensemble. For comparison the shear viscosity is also computed in the standard microcanonical NVE ensemble. A model that accurately reproduces the experimental vapor–liquid coexistence curve is shown to yield excellent results for the shear viscosity at the state point under study. © *1995 American Institute of Physics.*

I. INTRODUCTION

Considerable effort has been devoted to the accurate prediction of transport properties, such as the shear viscosity, from microscopic models. Systematic calculations of the shear viscosity via equilibrium molecular dynamics have been proven to be very successful.[1–3] The most common approach is to utilize the Green–Kubo (GK) formulation for transport coefficients.[4,5] This allows the transport property of interest to be expressed as a time integral over a corresponding correlation function. The GK expression for the shear viscosity is given by the integral of the stress autocorrelation function (SACF),

$$\eta(t)=\frac{V}{kT}\int_0^t\langle P_{xy}(0)P_{xy}(t^*)\rangle dt^*. \tag{1}$$

Here P_{xy} is the xy component of the pressure tensor, V is the volume, k is Boltzmann's constant, and T is the temperature.

A common approach in simulations of complex fluids, like long-chain alkanes, has been to use the method of constraints for the internal degrees of freedom, e.g., bond bends and stretching modes.[2,3] This method provides the computational advantage of allowing a larger time step than that permissible for a fully flexible model. Another way to decrease cpu time is to utilize only the repulsive part of the intermolecular potential [i.e., Weeks–Chandler–Anderson (WCA) potential] as the force-field between the molecules.[3] The main disadvantage of the WCA approach is that it is incapable of describing the vapor–liquid equilibria of the system under investigation and therefore fails to yield quantitative comparison with experimental data.

Our approach is to use models which can accurately predict the thermodynamic properties of the fluids to calculate the shear viscosity. Our goal is to predict *both* the critical properties and the transport properties of a molecular fluid within the same model. Furthermore, we wish to use a fully-flexible (including stretches, bends, and torsions) model for the alkane. To aid in computational efficiency we take advantage of a reversible form of the reference system propagator algorithm (RESPA).[6] This allows us to systematically divide the problem into the fast and slow time scales, each of which are handled with an appropriate time step. RESPA is able to achieve computational speed-ups by a factor of more than 2 in most cases. In this initial application for decane, comparisons are made between conventional simulations in the microcanonical ensemble (NVE), RESPA simulations in the canonical ensemble (NVT) and with experimental data.

II. THE MODEL

The interaction model used to describe *n*-decane has been derived by fitting to thermodynamic properties. Configurational-bias Monte Carlo calculations in the Gibbs ensemble were used to calculate the coexistence curves and critical properties of *n*-alkanes ranging from pentane to octatetracontane.[7,8] It was found that the united-atom approach in which methylene- and methyl-segment are treated as one *pseudo*-atom,[9] is sufficient to yield a very satisfactory description of the fluid phase diagram.[7] In Fig. 1, a comparison of the phase diagram of our model decane and experimental data are shown. In the model proposed in Ref. 7, pseudo-atoms in different molecules and those in the same molecule but separated by more than three CC bonds are assumed to interact through Lennard-Jones 12-6 potentials. The values of the Lennard-Jones parameters are $\sigma_{CH_3}=\sigma_{CH_2}=3.93$ Å, $\epsilon_{CH_3}=114$ K, and $\epsilon_{CH_2}=47$ K (Ref. 7) (where the parameters for the unlike interactions are calculated using $\epsilon_{ij}=\sqrt{\epsilon_i\epsilon_j}$). The nonbonded interactions are truncated at 3.5σ and the usual tail corrections have been employed to estimate the interactions beyond the cutoff (see next section). The beads in a given molecule are connected by rigid bonds ($d_{CC}=1.54$ Å). Bond bending is modeled by the harmonic potential proposed by van der Ploeg and Berendsen[10] and the torsional motion is governed by the potential of Jorgensen *et al.*[11]

For the molecular dynamics simulations presented here we made one minor modification to the model described above. The bond length is not anymore considered to be rigid and are now controlled by a harmonic potential with a force constant of 452 900 K/Å^2.[12] This modification has negligible influence on the phase diagram (see Fig. 1). At 475 K the coexistence densities for the model with fixed bond length are $\rho_L=0.574\pm0.01$ g/cm^3 and $\rho_V=0.010\pm0.002$

[a]Present address: Department of Chemistry, University of Minnesota, Minneapolis, MN 55455.

 0021-9606/95/102(8)/3376/5/$6.00

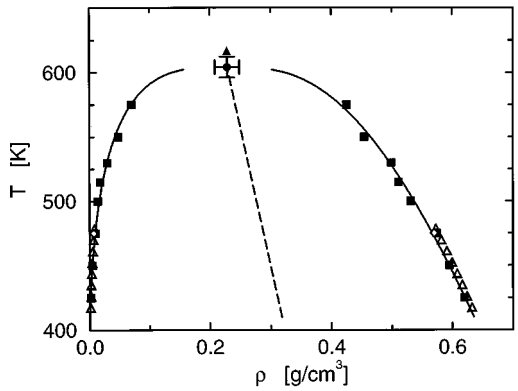

FIG. 1. Vapor–liquid curve of decane. Simulations from Ref. 7 are represented by filled squares and triangles for the coexistence densities and the critical point, respectively. An additional simulation for the fully flexible model used in the work presented here is also shown (open diamond, $T=475$ K). The experimental coexistence densities and critical point (Ref. 23) are pictured as open and filled triangles, respectively.

g/cm^3, and for the model used here $\rho_L=0.570\pm0.008$ g/cm^3 and $\rho_V=0.007\pm0.002$ g/cm^3. The small affect of the bond flexibility is in line with our previous observation that the use of a different torsional potential has an insignificant influence.[8]

III. SIMULATION DETAILS

The state point $T=480$ K and $\rho=0.6136$ g/cm^3 has been selected for all of our simulations on 64 molecules in a cubic simulation box of length 29.1 Å. A total of six independent simulations were carried out (i.e., starting from different well equilibrated initial configurations). Three in the standard microcanonical ensemble (NVE) and three using a reversible form of RESPA in the canonical ensemble (NVT-RESPA). Each of the six configurations were initially equilibrated from independent configurational-bias Monte Carlo calculations. A reversible Nosé–Hoover Chains (NHC) algorithm[13,19] was used to control the temperature in the latter case. A single NHC of length five coupled to all degrees of freedom was used throughout the NVT runs. Recall that the NHC masses are defined by the relation $Q_i=g_ikT\tau^2$. Here the ith thermostat in the chain is coupled to g_i degrees of freedom. The thermostating time constant, τ was set to 5 ps for the simulations reported here. A brief review of the reversible method of NHC is given in Appendix A.

In the case of the RESPA runs, all of the intramolecular potentials were considered to represent the ''fast'' time scales and the LJ intermolecular potential was considered the ''slow'' time scale. With this division we were able to choose the outer time step (slow) for the NVT-RESPA algorithm to be 3 fs with an inner (fast) time step of 1 fs. Each NVT-RESPA run consisted of 300 000 (outer) time steps corresponding to 900 ps. The pressure tensor data needed for the GK relation was collected every 3 fs. We found that this high frequency of data collection was instrumental to guarantee proper cancellation of the oscillations in the SACF. For a brief review of the technical details for the NVT-RESPA algorithm the interested reader should consult Appendix B.

TABLE I. Summary of the results of the NVE and NVT-RESPA simulations. The statistical errors of single runs in the temperatures and pressures have been estimated by the method of block averages. No statistical uncertainty for a single run has been obtained for the viscosities due to poor statistics. The final values are obtained as weighted averages from the three single runs. The last column gives the range of the experimental viscosity (Ref. 15) for the range in P,T-space estimated from the simulations.

	T/(K)	P/(atm)	η/(10^{-6} Pa s)	η_{exp}/(10^{-6} Pa s)
NVE_1	471.7±0.3	119± 9	210	
NVE_2	473.4±0.3	164±10	180	
NVE_3	478.4±0.3	204±11	320	
NVE	475.5±2	162±20	235 ± 40	209−232
NVT_1	481.2±1	190±10	225	
NVT_2	482.7±1	155±12	175	
NVT_3	479.7±1	159±10	165	
NVT	481.2±0.5	168±10	190 ± 15	201−214

The total run time of the NVE runs were 450 ps with a time step of 1 fs. This length was chosen so that a comparison of the calculated viscosity would be under the conditions of approximately equal cpu time. Pressure tensor data for the NVE runs were collected every time step. Long-range corrections[5] were employed to compute the internal pressure. The value of the correction term is -63 atm for the density and cutoff radius used in all runs.

The analysis of the pressure tensor can be completed by two methods. The first is the more common and takes advantage of isotropic symmetry. Because there is no preferred direction of shear in the simulation each of the off-diagonal components of the pressure tensor can be used to compute the correlation function in Eq. (1). The second method proposed by Evans[3] and derived using the principals of linear-irreversible thermodynamics,[4,14] once again takes advantage of the isotropic symmetry but makes use of the *full* pressure tensor which allows for improved statistics. This generalized GK formula for the shear viscosity is given by[3]

$$10\,\eta=\frac{V}{kT}\int_0^\infty dt\langle \mathrm{Tr}[\tilde{\mathbf{P}}(t)\tilde{\mathbf{P}}(0)]\rangle. \tag{2}$$

Here $\tilde{\mathbf{P}}$ is the symmetric traceless part of the full pressure tensor.

IV. DISCUSSION

The results for the calculated temperature and pressure for the six independent runs are given in Table I. It can be seen from Table I that the temperatures for the NVE simulations do not drift over the coarse of the simulation and stay close to 480 K. The thermostated temperatures fluctuate around 480 K, as expected.

The running integral of the viscosity the three individual NVE simulations [Eq. (1)] are given in Fig. 2. The corresponding results for the three individual NVT-RESPA runs are given in Fig. 3. The calculated viscosity for the NVT-RESPA runs appear to be significantly more converged than those for the NVE runs. This is to be expected since the NVT-RESPA calculations are a factor of 2 longer. It is also clear that any correlation function should be independent of

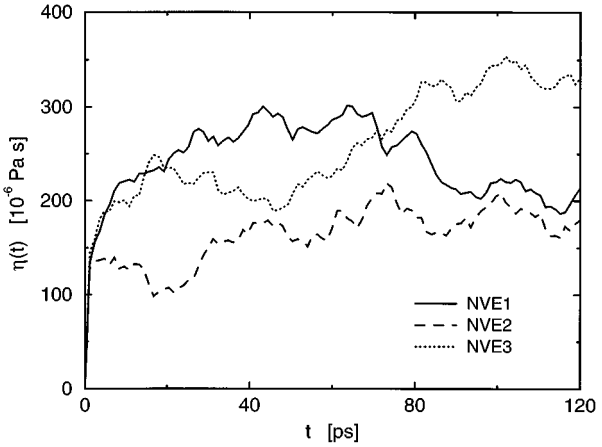

FIG. 2. The running intergal of the viscosity [Eq. (1)] as a function of time for the NVE simulations. The solid curve, long dash, and dotted curves are labeled NVE_1, NVE_2, and NVE_3 in Table I.

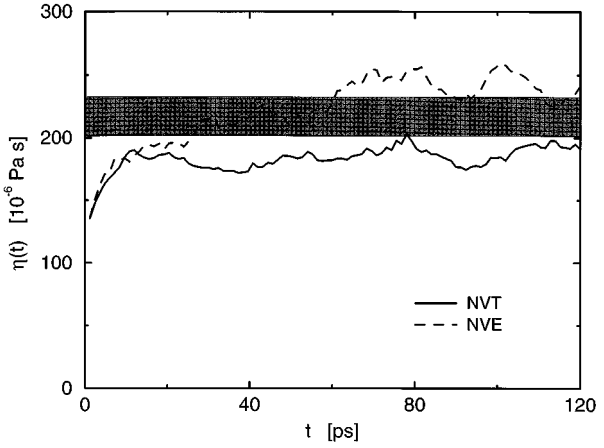

FIG. 4. The average running integral of the viscosity for NVT (solid), and NVE (long dash) simulations. The shaded area is the possible range of experimental values for the shear viscosity (Ref. 15) in the $P-T$ plane defined by the statistical uncertainties in the pressure of the simulations (see Table I).

initial conditions (for a specific state point). This is indeed the case for the results in Figs. 2 and 3 up to ~5 ps. Thereafter the correlations and the corresponding integrals diverge from each other partially due to poorer statistics. However, when averaging over the three independent results for the NVE and NVT-RESPA a much better estimate of the true correlation function can be obtained (see Fig. 4 and Table I). The experimental values[15] for the viscosities at the appropriate temperature and pressure are also given in Table I. As is evident from Fig. 4 and Table I, the potential model used in this study yields essentially quantitative agreement with the experimental data. To our knowledge, simulation results of this quality have not yet been obtained for complex fluids. Therefore we feel encouraged to continue our effort to fit potential models for the liquid state to experimental data taken from vapor–liquid equilibria.

One point of concern that should be discussed is our choice of thermostating time constant $\tau=5$ ps. We have also performed simulations with thermostating time constants of 500 and 50 fs. These choices give better temperature control (as expected), the same pressures, and the same diffusion constants within statistical uncertainties. Therefore, it would seem reasonable to assume the *equilibrium* properties of fluid decane have not been altered to any significant degree by the NHC. However, the degree of convergence of the SACF seems to be better with the slower thermostating time constants. More precisely, in the case of $\tau=50$ fs the running integral of the viscosity is in very good agreement with $\tau=5$ ps up to ~40 ps and reaches a very similar plateau value (see Fig. 5). Thereafter, the running integral seems to drift from the plateau region (see Fig. 5). For a thermosating time constant of $\tau=500$ fs the result, once again, seems well converged (see Fig. 5).

This is a subtle and puzzling issue. Earlier systematic studies of the effects of thermostating constants, τ, on other systems (e.g., Stockmayer fluids and proteins) showed no

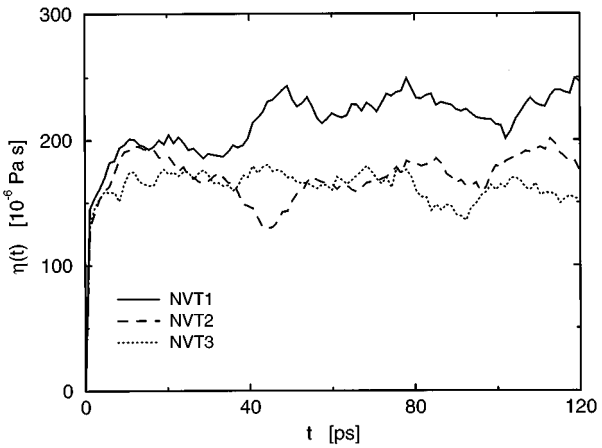

FIG. 3. The running integral of the viscosity [Eq. (1)] as a function of time for the NVT simulations. The solid curve, long dash, and dotted curves are labeled NVT_1, NVT_2, and NVT_3 in Table I.

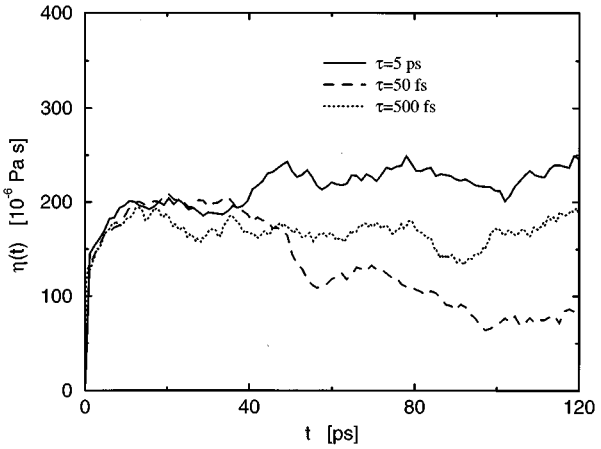

FIG. 5. The running integral of the viscosity for a NVT-RESPA run with $\tau=5$ ps (solid), $\tau=50$ fs (long dash), and $\tau=500$ fs (dotted). Note the agreement up to ~40 ps.

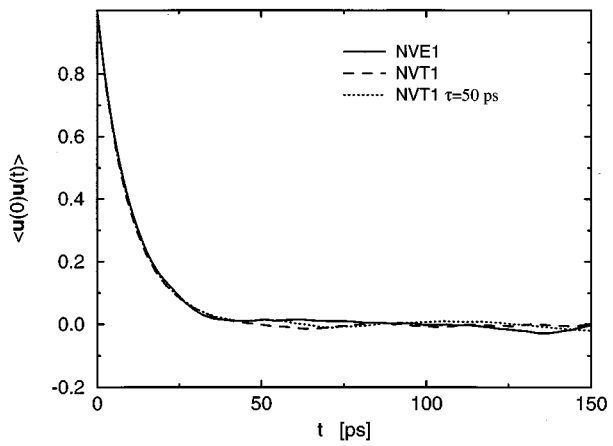

FIG. 6. The OAC for NVE1 (solid curve), NVT1 (long dash curve), and a NVT-RESPA run with $\tau=50$ fs (dotted curve). Here, **u** is the end-to-end vector of the alkane (see text).

discernible effect on the structural properties or velocity autocorrelation functions (VAC).[16,17] However, the effects on the zero-frequency mode of the autocorrelation function were not addressed in these studies. It is the zero frequency mode of the autocorrelation functions that determine the GK integral. It is also interesting to examine the effects of the thermostating on a mode with a long characteristic time. The reorientational relaxation of molecular fluids, in general, exhibit relaxation on longer time scales ($\sim$10–100 ps). We have compared the orientation autocorrelation function (OAC) for NVE1, NVT1 (see Table I) and a NVT-RESPA simulation with thermostating time constant $\tau=50$ fs in Fig. 6. It is interesting to note that the thermostat has a small effect on this property. Because the decay of the OAC is on the order of 40 ps, it is then imperative to sample this time scale with appropriate statistics in order to achieve a converged value of the viscosity (or any other transport property).[18] This is indeed the case in our study, and therefore seems likely that the difference appearing in Fig. 5 is not soley a problem due to poor statistics. We have also performed a shorter test run in the canonical ensemble (maintained with Nosé–Hoover thermostats) but without RESPA and detected the same problem as for the NVT-RESPA runs. Therefore, we believe that we can exclude RESPA as the source of the problem.

Clearly, a systematic study of the influence of thermostats on transport properties (perhaps starting with simpler model fluids) is desirable, but beyond the scope of this study. Therefore, we can only advise the reader to be aware of the problem and choose a relatively slow thermostating constant.

V. CONCLUSIONS

Three main conclusions emerge from our simulation study of the shear viscosity of decane. First, our model which was fitted to thermodynamic properties (e.g., the critical point of alkanes) yields a shear-viscosity in very good agreement with experiment. Next, the RESPA algorithm leads to a significant increase in computational efficiency and allows us to use fully flexible models. Finally, the influence of the thermostating frequency on the transport properties requires further study.

ACKNOWLEDGMENTS

Several stimulating and enlightening discussions with Kari Laasonen, Glenn Martyna, and Preston Moore are gratefully acknowledged. The work described herein was supported by the National Science Foundation and Albemarle Corporation. We thank Dixie Goins, Bill Moehle, Burney Lee, and Paul Kung for their encouragement.

APPENDIX A

The method of deriving reversible integrators is general and can be applied to all extended system Hamiltonians. In this Appendix a brief outline of the reversible NHC method[19] is given. The equations of motion which generate the canonical ensemble are[13]

$$\begin{aligned}
\dot{\mathbf{r}}_i &= \mathbf{p}_i\,,\\
\dot{\mathbf{p}}_i &= \mathbf{F}_i - \mathbf{p}_i\,\frac{p_{\xi_i}}{Q_i},\\
\dot{\xi}_i &= \frac{p_{\xi_i}}{Q_i},\\
\dot{p}_{\xi_1} &= \left(\sum_{i=1}^{N}\frac{\mathbf{p}_i^2}{m_i} - gkT\right) - p_{\xi_1}\frac{p_{\xi_2}}{Q_2},\\
\dot{p}_{\xi_j} &= \left(\frac{p_{\xi_{j-1}}^2}{Q_{j-1}} - kT\right) - p_{\xi_j}\frac{p_{\xi_{j+1}}}{Q_{j+1}},\\
\dot{p}_{\xi_M} &= \left(\frac{p_{\xi_{M-1}}^2}{Q_{M-1}} - kT\right).
\end{aligned} \tag{A1}$$

Here M is the length of the chain, N is the total number of particles, ξ and p_ξ the NHC position and momentum, and **F** is the total force. ξ, r, p, and p_ξ comprise the phase space $\mathbf{\Gamma}(t)$. To proceed reversibly, we consider the Liouvillian for the system,

$$iL_1 = \sum_{i=1}^{N}\left[\frac{\mathbf{F}_i(\mathbf{r})}{m_i}\right]\cdot\boldsymbol{\nabla}_{\mathbf{v}_i}, \tag{A2}$$

$$iL_2 = \sum_{i=1}^{N}\mathbf{v}_i\cdot\boldsymbol{\nabla}_{\mathbf{r}_i}, \tag{A3}$$

$$\begin{aligned}
iL_{\mathrm{NHC}} = &-\sum_{i=1}^{N} v_{\xi_1}\mathbf{v}_i\cdot\boldsymbol{\nabla}_{\mathbf{v}_i} + \sum_{i=1}^{M} v_{\xi_i}\partial\xi_i\\
&+ \sum_{i=1}^{M-1}(G_i - v_{\xi_i}v_{\xi_{i+1}})\partial v_{\xi_i} + G_M\partial v_{\xi_M}.
\end{aligned} \tag{A4}$$

Here, $G_1 = 1/Q_1\ (\Sigma_{i=1}^{N} m_i\mathbf{v}_i^2 - gkT)$ and

$$G_i = 1/Q_{i-1}(Q_{i-1}v_{\xi_{i-1}}^2 - kT)$$

for $i>1$. The total Liouvillian is defined as $iL = iL_1 + iL_2 + iL_{\mathrm{NHC}}$. It is also convenient to define the velocity Verlet (vV) operator as $iL_{vV} = iL_1 + iL_2$.

We can proceed to derive the equations of motion within the Trotter approximation.[20] Namely, for time step Δt we have

$$e^{iL\Delta t} = e^{iL_{\mathrm{NHC}}(\Delta t/2)} e^{iL_{vV}\Delta t} e^{iL_{\mathrm{NHC}}(\Delta t/2)} + O(\Delta t^3). \tag{A5}$$

The vV operator can be further broken down to yield

$$e^{iL_{vV}\Delta t} = e^{iL_1(\Delta t/2)} e^{iL_2\Delta t} e^{iL_3(\Delta t/2)} + O(\Delta t^3). \tag{A6}$$

By using the relation $e^{a\partial/\partial x} f(x) = f(x+a)$ the reversible algorithm can be derived. It should be noted, in some cases it is required to break up the iL_{NHC} operator using a multiple time step approach

$$e^{iL_{\mathrm{NHC}}(\Delta t/2)} = \prod_{i=1}^{n_c} e^{iL_{\mathrm{NHC}}(\Delta t/2n_c)}, \tag{A7}$$

where n_c is the number of multiple time steps. This may seem like a lengthy procedure, however one can integrate $e^{iL_{\mathrm{NHC}}(\Delta t/2)}$ with a higher-order integration algorithm[21,22] which results in a substantial reduction in n_c. The interested reader should consult the original Ref. 19.

APPENDIX B

In this Appendix we briefly discuss the technical aspects of the NVT-RESPA algorithm.[6,19] The basic idea behind RESPA is to break up the operator $e^{iL_{vV}\Delta t}$ into a part containing the reference (intramolecular) force and what remains (intermolecular force) such that

$$\mathbf{F}_i = \mathbf{F}_i^{\mathrm{ref}} + d\mathbf{F}_i. \tag{B1}$$

We now apply a multiple time step procedure to Eq. (A5) to yield

$$(e^{iL(\Delta t/n)})^n = (e^{iL_{\mathrm{NHC}}(\Delta t/2n)} e^{iL_{vV}(\Delta t/n)} e^{iL_{\mathrm{NHC}}(\Delta t/2n)})^n. \tag{B2}$$

The operator iL_{vV} can be broken down further giving

$$\begin{aligned} iL_{vV} &= iL_{\mathrm{ref}} + iL_{dF}, \\ iL_{\mathrm{ref}} &= \mathbf{v}_i \cdot \nabla_{\mathbf{r}_i} + \frac{\mathbf{F}_i^{\mathrm{ref}}}{m_i} \cdot \nabla_{\mathbf{v}_i}, \\ iL_{dF} &= \frac{d\mathbf{F}_i}{m_i} \cdot \nabla_{\mathbf{v}_i}. \end{aligned} \tag{B3}$$

The Trotter approximation is then used to construct the total operator where there are $n-2$ applications of the following operator on Γ:

$$O_1 O_2 O_3 O_2 O_1, \tag{B4}$$

and the first and last time step of the multiple time step procedure use the operator

$$O_1 O_4 O_3 O_2 O_1, \tag{B5}$$

with

$$\begin{aligned} O_1 &= \exp\left(iL_{\mathrm{NHC}} \frac{\Delta t}{2n} \right), \\ O_2 &= \exp\left(\frac{\Delta t}{2n} \frac{\mathbf{F}_i^{\mathrm{ref}}}{m_i} \cdot \nabla_{\mathbf{v}_i} \right), \\ O_3 &= \exp\left(\frac{\Delta t}{n} \mathbf{v}_i \cdot \nabla_{\mathbf{r}_i} \right), \\ O_4 &= \exp\left[\frac{\Delta t}{2n} \left(\frac{n d\mathbf{F}_i}{m_i} + \frac{\mathbf{F}_i^{\mathrm{ref}}}{m_i} \right) \cdot \nabla_{\mathbf{v}_i} \right]. \end{aligned} \tag{B6}$$

[1] G. Maréchal and J.-P. Ryckaert, Chem. Phys. Lett. **101**, 548 (1983).
[2] G. Maréchal, J.-P. Ryckaert, and A. Bellemans, Mol. Phys. **61**, 33 (1987).
[3] P. J. Davis and D. J. Evans, J. Chem. Phys. **100**, 541 (1994).
[4] D. J. Evans and G. P. Morriss, *Statistical Mechanics of Nonequilibrium Liquids* (Academic, New York, 1990).
[5] M. P. Allen and D. J. Tildesley, *Computer Simulation of Liquids* (Oxford University, Oxford, 1987).
[6] (a) M. E. Tuckerman, B. J. Berne, and G. J. Martyna, J. Chem. Phys. **97**, 1990 (1992); (b) D. D. Humphreys, R. A. Friesner, and B. J. Berne, J. Phys. Chem. **98**, 6885 (1994).
[7] J. I. Siepmann, S. Karaborni, and B. Smit, Nature **365**, 330 (1993).
[8] B. Smit, S. Karaborni, and J. I. Siepmann, J. Chem. Phys. (submitted).
[9] J. P. Ryckaert and A. Bellemans, Chem. Phys. Lett. **30**, 123 (1975).
[10] P. van der Ploeg and H. J. C. Berendsen, J. Chem. Phys. **76**, 3271 (1982).
[11] W. L. Jorgensen, J. D. Madura, and C. J. Swenson, J. Am. Chem. Soc. **106**, 6638 (1984).
[12] W. E. Reiher, Ph.D. thesis, Harvard University, Cambridge, Massachusetts, 1985.
[13] G. J. Martyna, M. L. Klein, and M. E. Tuckerman, J. Chem. Phys. **97**, 2635 (1992).
[14] S. R. deGroot and P. Mazur, *Non-equilibrium Thermodynamics* (Dover, New York, 1984).
[15] K. Stephan and K. Lucas, *Viscosity of Dense Fluids* (Plenum, New York, 1979).
[16] V. A. Payne, M. Forsyth, J. Kolafa, M. A. Ratner, and S. W. de Leeuw, J. Phys. Chem. **97**, 10 478 (1993).
[17] D. J. Tobias, G. J. Martyna, and M. L. Klein, J. Phys. Chem. **97**, 12 959 (1993).
[18] M. K. Hounkonnou, C. Pierleoni, and J.-P. Ryckaert, J. Phys. Chem. **97**, 9335 (1992).
[19] G. J. Martyna, D. J. Tobias, M. L. Klein, and M. E. Tuckerman (preprint, 1994).
[20] A. F. Trotter, Proc. Am. Math. Soc. **10**, 545 (1959).
[21] H. Yoshida, Phys. Lett. A **150**, 260 (1990).
[22] M. Suzuki, J. Math. Phys. **32**, 400 (1991).
[23] M. J. Anselme, M. Gude, and A. S. Teja, Fluid Phase Equilibria **57**, 317 (1990).